Solution NMR Characterization of the Thermodynamics of the Disulfide Bond Orientational Isomerism and Its Effect of Cluster Electronic Properties for the Hyperthermostable Three-Iron Cluster Ferredoxin from the Archaeon *Pyrococcus furiosus*†

Mateus Webba da Silva,‡ Simon Sham,‡ Carol M. Gorst,‡ Luigi Calzolai,‡ Philip S. Brereton,§ Michael W. W. Adams,§ and Gerd N. La Mar*,‡

Department of Chemistry, University of California, Davis, Davis, California 95616, and Department of Biochemistry and Molecular Biology, Center for Metalloenzyme Studies, University of Georgia, Athens, Georgia 30602

Received March 28, 2001; Revised Manuscript Received July 19, 2001

ABSTRACT: The thermodynamics and dynamics of the Cys21−Cys48 disulfide "*S*" ⇔ "*R*" conformational isomerism in the three-iron, single cubane cluster ferredoxin (Fd) from the hyperthermophilic archaeon *Pyrococcus furiosus* (*Pf*) have been characterized by ^{1}H NMR spectroscopy in both water and water/methanol mixed solvents. The mean interconversion rate at 25 °C is 3×10^3 s^{-1} and $\Delta G_{298} = -0.2$ kcal/mol [$\Delta H = 4.0$ kcal/mol; $\Delta S = 14$ cal/(mol·K)], with the *S* orientation as the more stable form at low temperature (<0 °C) but the *R* orientation predominating at >100 °C, where the organism thrives. The distinct pattern of ligated Cys β-proton contact shifts for the resolved signals and their characteristic temperature behavior for the forms of the 3Fe Fd with alternate disulfide orientations have been analyzed to determine the influences of disulfide orientation and methanol cosolvent on the topology of the inter-iron spin coupling in the 3Fe cluster. The Cys21−Cys48 disulfide orientation influences primarily the spin couplings involving the iron ligated to Cys17, whose carbonyl oxygen is a hydrogen bond acceptor to the Cys21 peptide proton. Comparison of the Cys β-proton contact shift pattern for the alternate disulfide orientations with the pattern exhibited upon cleaving the disulfide bridge confirms an earlier [Wang, P.-L., Calzolai, L., Bren, K. L., Teng, Q., Jenney, F. E., Jr., Brereton, P. S., Howard, J. B., Adams, M. W. W., and La Mar, G. N. (1999) *Biochemistry 38,* 8167−8178] proposal that the structure of the same Fd with the *R* disulfide orientation resembles that of the Fd upon cleaving the disulfide bond.

The bacterial-type ferredoxins (Fds)[1] are small (6−10 kDa) electron-transfer proteins that possess one or two cubane 4Fe and/or 3Fe clusters (*1*−*3*). A schematic representation for a typical one-cluster Fd is depicted in Figure 1. The prevailing interpretive basis (*4*−*10*) of the unusual electronic/magnetic properties of these clusters involves valence delocalization between pairs of irons as an intrinsic cluster property for which the final, antiferromagnetically coupled spin ground state, S_T, for the different cluster oxidation states is generated from the coupling of the spins of the two valence-delocalized iron pairs, $\vec{S}_A$ and $\vec{S}_B$, spin vectors, via $\vec{S}_A + \vec{S}_B = S_T$. Thus the reduced (*4*, *8*, *10*) 4Fe Fd^{red} = [4Fe:4S]$^{1+}$ with 2Fe$^{2.5+}$ ($S_A = {}^9/_2$); 2Fe$^{2.0+}$ ($S_B = 4$) yields $S_T = {}^1/_2$, and the oxidized 4Fe Fd^{ox} = [4Fe:4S]$^{2+}$ with 2Fe$^{2.5+}$ ($S_A = {}^9/_2$); 2Fe$^{2.5+}$ ($S_B = {}^9/_2$) yields $S_T = 0$. For the 3Fe Fd^{red} = [3Fe:4S]^0, with 2Fe$^{2.5+}$($S_A = {}^9/_2$); 1Fe$^{3.0+}$ ($S_B = {}^5/_2$), yields $S_T = 2$ (*5*), and

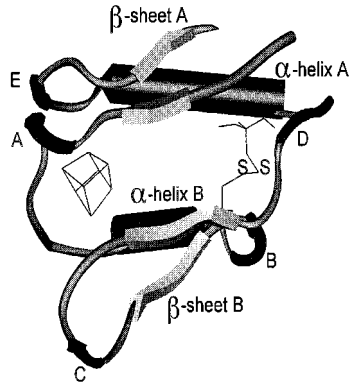

FIGURE 1: Schematic representation of the molecular structure of a single cubane cluster Fd that possesses two α-helices (A and B), two β-sheets (A and B), five turns (A−E), a cubane cluster, and a disulfide bond. The model is based on the *Tm* Fd crystal structure (*33*).

3Fe Fd^{ox} = [3Fe:4S]$^{1+}$ where, although all three irons are ferric, the observed $S_T = {}^1/_2$ ground state is rationalized by a 1Fe$^{3.0+}$ ($S = {}^5/_2$):2Fe$^{3.0+}$ ($S = 2$) coupling topology (*11*). There is currently considerable interest (*12*−*14*) in the molecular structural basis of the electron-transfer rate and the overall cluster potential as well as the micropotentials of the iron pairs that determine the location(s) in the protein matrix of the "reducing" electron in either 3Fe or 4Fe Fd^{red}.

† This work was supported by Grants MCB96-00759 (G.N.L.) and MCB99-04624 (M.W.W.A.) from the National Science Foundation.

* Address correspondence to this author. Phone: (530) 752-0958. Fax: (530) 752-8995. E-mail: lamar@indigo.ucdavis.edu.

‡ University of California.

§ University of Georgia.

[1] Abbreviations: Fd, ferredoxin; *Pf*, *Pyrococcus furiosus*; *Tl*, *Thermococcus litoralis*; *Tm*, *Thermatoga maritima*; DSS, 2,2-dimethyl-2-silapentane-5-sulfonate; EXSY, two-dimensional exchange spectroscopy; TOCSY, two-dimensional total correlation spectroscopy; NOESY, two-dimensional nuclear Overhauser spectroscopy.

10.1021/bi0106179 CCC: $20.00
Published on Web 10/02/2001

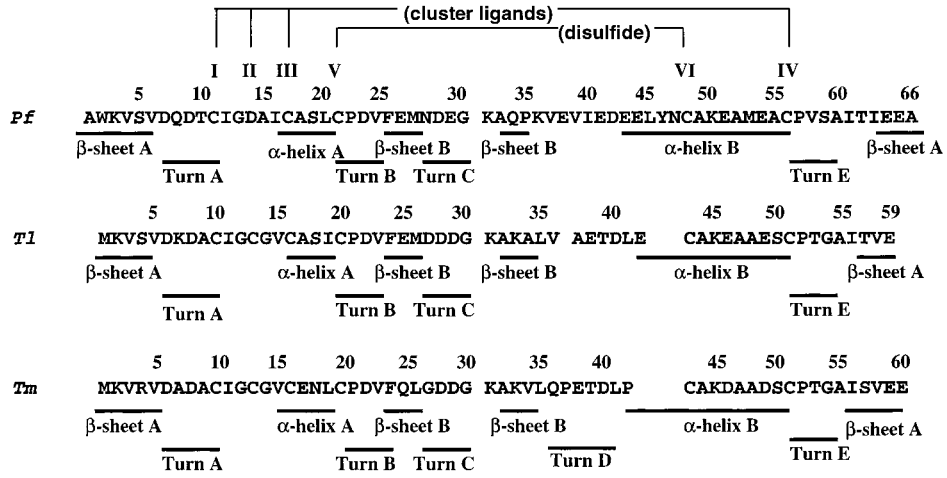

FIGURE 2: Amino acid sequence alignment of the ferredoxins from *P. furiosus* (*Pf*), *T. maritima* (*Tm*), and *T. litoralis* (*Tl*). The ligands in the cluster ligating consensus sequences are single cubane clusters labeled I−IV, and the two Cys involved in the disulfide bond are labeled V and VI. The positions of conserved secondary structural elements (*21*, *22*, *29*, *33*, *58*, *59*) are provided below each of the sequences.

Crucial to these investigations are the elucidation of which of the pair of irons in the cluster is the site of the electron "storage" and the determination of the molecular structure of a variety of Fds.

NMR has made important contributions to the understanding of the molecular/electronic structure (*10*, *15*−*18*) of cubane cluster Fds. On one hand, it has provided solution molecular structures (*19*−*26*) in several cases that complement the more common approach by X-ray crystallography (*27*−*35*). On the other hand, NMR is unique in its ability to identify the oxidation states of the individual iron atoms by the characteristic temperature dependence of the contact shifts for the ligated Cys protons (*10*, *24*, *36*−*46*) (or other ligand) (*41*, *44*), which is given by (*10*, *47*)

$$\delta^{q}_{con}(C_{\beta}H) = -\langle S_z\rangle_q A_q B_o f(\theta) \qquad (1)$$

where A_q is a measure of the delocalized spin density on a ligand to iron q, $f(\theta)$ is the function that depends on the Fe−S−C_β−H dihedral angle, θ, $\langle S_z\rangle_q$ is the spin magnetization on iron q, and B_o is the magnetic field in the cluster. In the antiferromagnetic coupling of the $\vec{S}_A$ and $\vec{S}_B$ pairs which yields S_T, the larger S_A will necessarily exhibit low-field δ_{con} with a positive slope in a Curie plot (increasing shifts with decreasing temperature or Curie-like), while the ligand to the iron pair B with the smaller S_B, at least for the [4Fe:4S]$^{1+}$ cluster, will tend to exhibit low-field δ_{con} but with negative slope or anti-Curie (increasing shift with increasing temperature) slope due to a negative $\langle S_z\rangle$ at low temperature (*10*). Thus 4Fe Fd^{red} invariably exhibits two ligated Cys with Curie-like, and two ligated Cys with anti-Curie-like temperature dependence (*10*, *15*, *36*−*38*, *42*, *44*, *48*−*50*) of δ_{con}. For the 3Fe Fd^{ox} [NMR spectra of cluster ligand protons of 3Fe Fd^{red} have either not been observed (*51*) or not analyzed (*36*, *52*)] one iron ligand exhibits Curie-like (*53*−*56*) and the other two anti-Curie-like (*52*, *55*, *56*) temperature dependence, consistent with the larger S_A for the single iron.

The single cubane cluster Fd from the hyperthermophile archaeon *Pyrococcus furiosus* (*Pf*) possesses several properties that distinguish it not only from the Fds of mesophiles but from Fds of other characterized hyperthermophiles as well. In common with the Fd from other hyperthermophiles, *Pf* Fd provides a candidate for elucidating the structural basis of the extraordinary thermostability (*21*, *33*, *57*−*59*) in relatively small proteins. Moreover, *Pf* Fd possesses a unique Asp14 (Figure 2) as one of its cluster ligands in its native 4Fe state (*41*), which significantly affects the electron exchange rate (*60*) and allows facile interconversion between 4Fe and 3Fe forms (*61*). Last, in contrast to other hyperthermostable Fds, the *Pf* Fd disulfide bond is reducible at the same potential as the cluster (*62*). Structural characterization of *Pf* Fd by crystallography has not been successful, and cocrystallization of the Fd with its tungsten-containing oxidoreductase revealed (*63*) a resolved Fd cluster in contact with the enzyme but a disordered remainder of the Fd structure. Thus solution ^{1}H NMR studies have been initiated to elucidate both the cluster electronic properties (*41*, *44*, *55*, *60*) and the solution molecular structure (*40*, *58*, *59*).

One unique, but disadvantageous, property of *Pf* Fd, however, detected earlier (*55*, *60*) but only recently characterized, is that any form of the *Pf* Fd with an intact disulfide bond (*62*) (see Figures 1 and 2) between Cys21(V) and Cys48(VI) exhibits a dynamic, equilibrium structural heterogeneity (*59*). Thus the contact-shifted cluster ligand C_β-Hs (*55*, *60*) and numerous protein peptide NHs exhibit extreme line broadening at low temperature in all forms with intact disulfide bond (*59*). Qualitative characterization of the secondary structural elements in *Pf* Fd shows (*58*, *59*) that its sequence extensions relative to other (*21*, *22*, *29*, *33*) Fds (see Figure 2) are in the form of a one-turn extension of helix B and 1−2 residue extension of β-sheet A in contact with this helix (see Figures 1 and 2), which destabilizes (*59*) the common *S* orientation disulfide bond relative to the *R* orientation. The alternative *R* and *S* orientations of the disulfide bond represent left- and right-handed helical disposition of the C_α−C_β−S−S−C_β−C_α atoms, as depicted in Figure 3. The "*S*" or right-handed form is more stable and is the only form found in all other Fds (*21*−*23*, *29*, *33*). This destabilization of the common disulfide *S* orientation rationalizes (*59*) the facile reduction of the disulfide bond in *Pf* Fd (*62*) relative to other hyperthermostable Fds (*21*, *33*). A preliminary molecular model[2] of *Pf* 4Fe Fd_A^{ox} confirms the comparable stabilities of the disulfide *S* and *R*

[2] S. Sham, P.-L. Wang, L. Calzolai, M. W. W. Adams, and G. N. La Mar, manuscript in preparation.

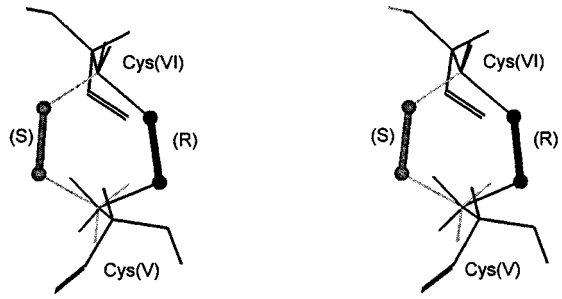

FIGURE 3: Stereoviews of the alternate [*S* (shaded) or *R* (dark)] orientations of the disulfide bond between Cys(V) and Cys(VI) in single cubane cluster Fds. The right-handed or *S* orientation is observed in all structurally characterized Fds (*21*, *22*, *29*, *33*).

conformations. The pattern of line broadening observed in numerous residues over the molecule suggests (*59*) a global rather than local structure accommodation to the disulfide orientation, which may account for the disorder observed in crystals (*63*).

In this report we are interested in further characterization of the structural heterogeneity of *Pf* Fd to determine if it is functionally relevant at the physiological temperature >100 °C. Moreover, because there is a direct link between the disulfide and cluster redox chromophores in the form of a hydrogen bond for the Cys21(V) peptide NH to the cluster-bound Cys17(III) carbonyl oxygen in all structurally characterized single-cluster Fds (*21*, *29*, *33*), we seek to define how the cluster magnetic coupling topology, as manifested in the magnitudes of the contact shifts of the cluster ligands and their characteristic temperature dependence, is influenced by the disulfide bond orientation. Last, to assess the potential utility of nonaqueous solvents in order to extend the liquid range of solution studies of *Pf* Fd, we explore the influence of methanol on the solution structure and cluster magnetic properties well below 0 °C. Analysis of the effect of cluster architecture (3Fe vs 4Fe) and Asp14Cys mutation has shown that the disulfide orientational heterogeneity is present to essentially the same degree in each of the three cluster forms (*59*). However, only in the 3Fe Fd^{ox} form is it possible to resolve the ligand peaks of the two contributing forms (*55*), and hence it allows the characterization of the thermodynamics of the heterogeneity by simple resonance intensity comparison.

EXPERIMENTAL PROCEDURES

Proteins. The gene encoding of *Pf* Fd was expressed in *Escherichia coli* and then was purified as the four-iron reduced cluster (superscript red) form with free thiols for Cys21(V) and Cys48(VI) (subscript B), i.e., *Pf* 4Fe Fd_B^{red}, as described in detail previously (*64*). The isolated 4Fe Fd_B^{ox} was converted either completely to 3Fe Fd_A^{ox} [oxidized cluster, disulfide bridge between Cys21(V) and Cys48(VI)] by aerobic addition of excess ferricyanide (*61*) or partially to 3Fe Fd_B^{ox} [oxidized cluster but still free thiols for Cys21-(V) and Cys48(VI)] by the anaerobic titration with ferricyanide until ~30% conversion to 3Fe Fd_B^{ox} and a remaining ~70% 4Fe Fd_B^{ox}, as described in detail previously (*62*). The amount of 3Fe Fd_A^{ox} or 4Fe Fd_A^{ox} generated was negligible (<5%). Protein samples were prepared to a final concentration of ~8 mM (Fd_A^{ox}) and ~2 mM (Fd_B^{ox}) in ^1H_2O, 50 mM in phosphate and pH 8.0, and 10% ^2H_2O was added to provide the NMR lock. Methanol was titrated into the WT 3Fe Fd_A^{ox} sample in increments to 30%/70% v/v methanol/water.

NMR Spectra. ^{1}H NMR spectra were recorded on either a GE Omega-500 or a Bruker AVANCE-600 spectrometer operating at 500 and 600 MHz, respectively. Variable temperature reference spectra at 600 MHz over the range 90 to −18 °C were collected over a 40 kHz bandwidth at a repetition rate of 3 s^{-1} using 4096 points and 5 Hz line broadening to characterize the hyperfine-shifted ligand resonance in the 10−30 ppm spectral window and over a 16 kHz bandwidth at a repetition rate of 0.33 s^{-1} using 16384 points and 1 Hz line broadening to characterize the resonance in the 0−10 ppm window which is relatively unaffected by the cluster paramagnetism. Chemical shifts are referenced to 2,2-dimethyl-2-silapentane-5-sulfonate (DSS) through the residual solvent signal(s).

EXSY spectra at 500 MHz (*65*) were recorded at low temperatures over a bandwidth 40 kHz with a mixing time of 1.5 ms using 512 t_1 blocks of 512 scans and 1024 t_2 points and a repetition rate of 10 s^{-1} to correlate resonances for the *S* and *R* forms of 3Fe Fd_A^{ox} in 70%/30% v/v water/methanol. TOCSY (*66*) (80 ms mixing time) and NOESY (*65*) (200 ms) spectra over the diamagnetic spectral window (bandwidth 16 kHz) were recorded on a sample of 3Fe Fd_A^{ox} in 70%/30% v/v water/methanol using 512 t_1 blocks of 64 scans and 2048 t_2 points recorded at a repetition rate of 1 s^{-1}. The 2D data were apodized by 30°-shifted sine-bell-squared functions and zero-filled to 2048 × 2048 data points prior to Fourier transformation.

The thermodynamics and dynamics of the disulfide orientational isomerism

$$3Fe\ Fd_A^{ox}(S) \underset{k_R}{\overset{k_S}{\rightleftharpoons}} 3Fe\ Fd_A^{ox}(R) \qquad (2)$$

were analyzed on the basis of the intensities and line widths of the two species over a temperature range 2−21 °C in water and −18 to 20 °C in 70%/30% v/v water/methanol of the optimally resolved split components of the low-field Cys11-(I) $C_\beta H'$ peak. The relative intensities were obtained by simulation of two Lorenzians arising from the *S* and *R* components of the $C_\beta H$ peaks and the equilibrium constant $K_{S\rightarrow R}$ and $\Delta G(S\rightarrow R)$, related by

$$\Delta G(S\rightarrow R) = RT \ln K_{S\rightarrow R} = RT \ln[Fd_A^{ox}(R)]/[Fd_A^{ox}(S)] \qquad (3)$$

were determined, where $[Fd_A^{ox}(R)]$ and $[Fd_A^{ox}(S)]$ are the intensities of the two respective components in arbitrary units. The $\Delta H(S\rightarrow R)$ and $\Delta S(S\rightarrow R)$ values were derived from the straight lines in a van't Hoff plot. The mean rate of the interconversion (*67*), $k = {}^1/_2(k_S + k_R)$, was obtained by solving the exchange matrix in the extended Bloch equation, as performed by the "Mex" program (*68*). Cys11(I) $C_\beta H$ line widths in the absence of exchange were estimated from the line width of the Cys11(I) $C_\beta H$ signal of 3Fe Fd_B^{ox}, which does not exhibit the dynamic equilibrium. Activation parameters were derived from Eyring and Arrhenius plots.

RESULTS

Resolution of the R- and S-Disulfide Isomer Signals. The assignment of the *R*-disulfide orientation to the species

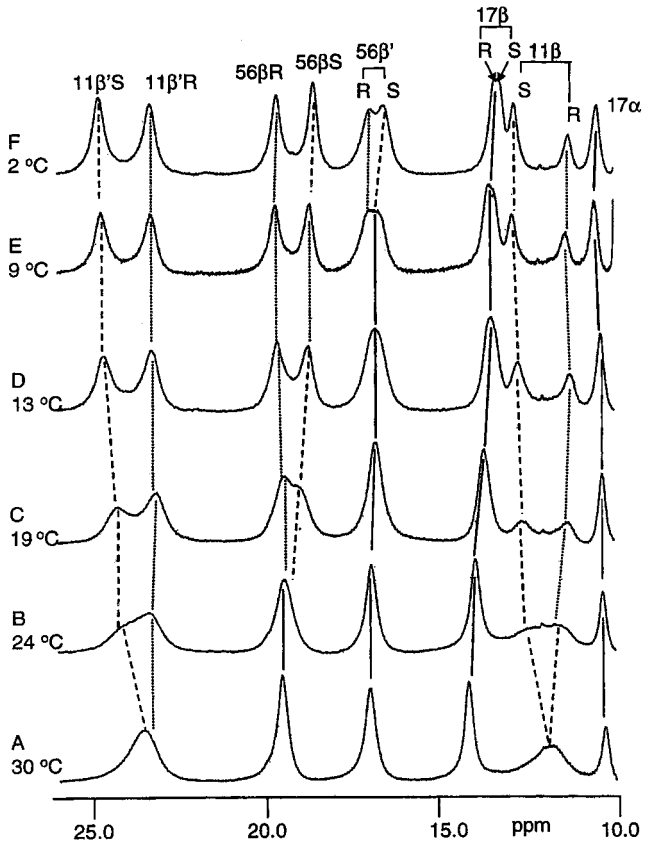

FIGURE 4: Low-field resolved portions of the 600 MHz ^{1}H NMR spectra of *Pf* 3Fe Fd_A^{ox} in ^1H_2O, 50 mM in phosphate, pH 8.2, over the temperature range 30−2 °C. The resonances are labeled at 2 °C as previously assigned where β and β' represent the Cys β proton further from, and closer to, the iron, respectively. Upon resolution of the two forms of the Fd below 20 °C, the less intense component at 2 °C is labeled by *R*, and the more intense by *S*, for each proton.

favored at elevated temperature was based on two observations for the "diamagnetic" portion of the ^{1}H NMR spectra (*21*). First, analysis of the temperature dependence of the NH chemical shifts for the residues remote from the cluster suggested that a single species dominated near 100 °C. Second, NOESY cross-peak intensities between Cys48 C_β-Hs and Leu45 C_αH (characteristic only of the "*R*" orientation) increased with temperature (*29*). The ^{1}H NMR spectrum of 3Fe Fd_A^{ox} at elevated temperatures exhibits six resolved, hyperfine-shifted and strongly relaxed signals for nonlabile protons previously assigned (*40*, *55*) to the two C_βHs for each of Cys11 (11β, 11β') and Cys56 (56β, 56β') and one C_βH (17β) and the C_αH (17α) of Cys17, as well as an unassigned, resolved peptide NH, as shown in Figure 4A; the more strongly relaxed β-proton, and hence closer to the iron, of the two β-protons is labeled β'. As the temperature is lowered, each of the Cys signals (except Cys17 C_αH) broadens and then splits into two signals, as reported previously (*55*). At 24 °C (Figure 4B), both the 11β and 11β' peaks split into a minor (labeled *S*; 11β_S) and a major (labeled *R*; 11β_R) peak. At 19 °C (Figure 4C), the Cys56 C_βH similarly splits into a minor (labeled *S*) and major (labeled *R*) peak. As the temperature is further lowered, the relative intensities of the Cys11 *R* and *S* peaks 11β'_S and 11β'_R invert, with those labeled *S* becoming the major component. Below 10 °C (Figure 4E), the Cys56 11β also

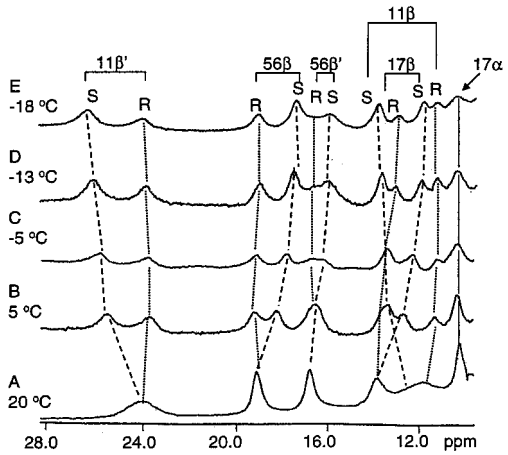

FIGURE 5: Low-field, resolved portions of the 600 MHz ^{1}H NMR spectra of *Pf* 3Fe Fd_A^{ox} in 70% ^1H_2O/30% C^2H_3OH, 50 mM in phosphate, pH 8.2, over the temperature range 20 to −18 °C. The resolved resonances are labeled at −18 °C, with split components of each resonance labeled by *S* or *R* for the more intense and less intense components at −18 °C, respectively.

splits, and the comparison to the relative intensities of the split Cys11 and Cys56 C_βH peaks allows unambiguous differentiation of the *S* and *R* components. At 2 °C in H_2O (Figure 4F), the Cys17 C_βH peak exhibits evidence of asymmetry, suggesting a splitting. It is notable that, for Cys11, the larger contact shifts are exhibited by the *S* component, while for Cys56, it is the *R* component which displays the larger contact shifts.

Influence of Methanol. Addition of methanol has minimal effects on the chemical shifts of the diamagnetic portion of the protein, as evidenced by essentially identical reference and 2D NOESY NMR spectra and only very small shift changes (≤0.02 ppm) for NHs (not shown; see Supporting Information) up to 30% v/v methanol. The effect of methanol on Cys C_βH shifts, however, is not negligible and will be considered below. The low-field portions of the 600 MHz ^{1}H NMR spectra of *Pf* 3Fe Fd_A^{ox} in 70%/30% v/v H_2O/methanol as a function of temperature are illustrated in Figure 5. While the chemical shifts for the various resonances, in particular those in the diamagnetic envelope, are similar in ^1H_2O and 70%/30% H_2O/CH_3OH, it requires a lower temperature by ∼10 °C to bring the spectra in the latter solvent to the same degree of dynamic resolution into the *R* and *S* components as in ^1H_2O. Thus, when the splitting occurs for all resonances at 5 °C in water/methanol, the *R* and *S* component peaks have comparable intensity (Figure 5B). However, upon lowering the temperature to −18 °C (Figure 5E), it is obvious that each split component results in one clearly more intense peak in each case. Moreover, below 0 °C, the Cys17(III) C_βH also resolves clearly into two components of unequal intensity, with the *R* component [like Cys56(IV)] exhibiting the larger contact shift.

Because of the spectral congestion and the need to determine individual chemical shifts for overlapping lines in the 10−15 ppm window below 0 °C (Figures 5C−E), it was necessary to cross-correlate the two components signals by 2D EXSY spectra (*65*), as illustrated in Figure 6B at −13 °C. This −13 °C map uniquely locates the *S*/*R* pairs for each resonance after each is resolved, and the relative intensities at −13 °C (Figure 6A) clearly differentiates the *S* and *R* sets of peaks. The chemical shifts of the individual peaks of

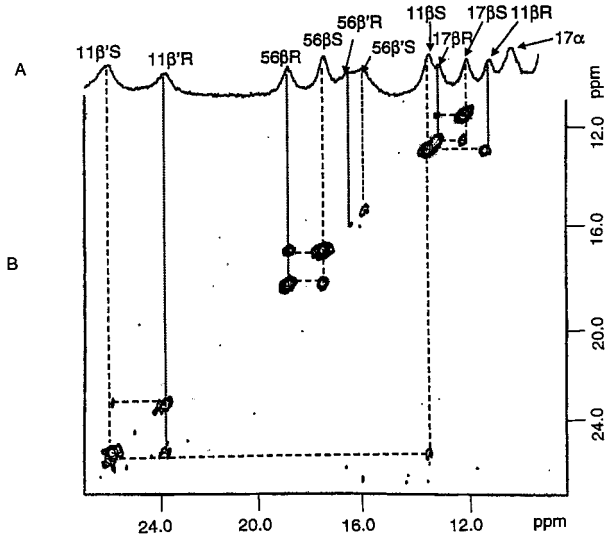

FIGURE 6: (A) Low-field 600 MHz ^{1}H NMR reference spectrum of 3Fe *Pf* Fd_A^{ox} in 70% ^1H_2O/30% v/v $^1H_2O/C^2H_3OH$, 50 mM in phosphate, at −13 °C where the resonances for the *R*- and *S*-disulfide orientation are resolved (peaks are labeled as in Figure 4). (B) 2D EXSY spectrum (2.5 ms mixing time at −13 °C) which establishes the connections between the *R* and *S* orientation peaks. Note that in each case the two components clearly have different intensities, with the less intense component labeled *R*.

Table 1: Influence of Temperature, Solvent, and Disulfide Bond Orientation on the Ligated Cys Contact Shifts in *Pyrococcus furiosus* Three-Iron Ferredoxin

			δ_{DSS}(obs)[a]					
			Cys11		Cys17		Cys56	
3Fe Fd	solvent	*T*, °C	$C_\beta H$	$C_\beta H'$	$C_\beta H$	$C_\alpha H'$	$C_\beta H$	$C_\beta H'$
Fd_A^{ox}	H_2O	30	23.60	11.89	14.19	10.27	19.64	17.06
Fd_A^{ox}	H_2O/CH_3OH	30	23.83	12.02	14.16	10.16	19.55	16.94
Fd_B^{ox}	H_2O	30	23.26	11.56	13.70	10.10	20.15	17.83
Fd_A^{ox}(*S*)	H_2O	5	24.84	12.83	13.32	10.48	18.71	16.64
Fd_A^{ox}(*R*)	H_2O	5	23.41	11.27	13.32	10.48	19.77	16.97
Fd_A^{ox}(*S*)	H_2O/CH_3OH	5	25.54	13.10	13.51	10.41	18.31	16.64
Fd_A^{ox}(*R*)	H_2O/CH_3OH	5	23.73	11.37	12.73	10.41	19.30	16.64
Fd_B^{ox}	H_2O	5	23.41	11.03	13.43		19.61	17.25
Fd_A^{ox}(*S*)	H_2O/CH_3OH	−18	26.49	9.18	13.20	10.56	18.71	16.61
Fd_A^{ox}(*R*)	H_2O/CH_3OH	−18	24.35	8.40	13.20	10.56	20.05	17.23

[a] Chemical shift in ppm referenced to DDS, in ^1H_2O or 70% H_2O/30% CH_3OH solution at pH ~8.2.

3Fe Fd_A^{ox} at 30 and 5 °C (in both solvents) and at −18 °C in H_2O/CH_3OH, are listed in Table 1.

Temperature Behavior of Cys $C_\beta H$ Contact Shifts. The Curie plot (observed chemical shift versus reciprocal absolute temperature) for the resolved Cys $C_\beta H$ resonances in H_2O (closed markers) and 70%/30% v/v $^1H_2O/CH_3OH$ (open markers) is illustrated in Figure 7. Upon splitting into two components, the markers are distinguished for the *S* and *R* components. The influence of methanol addition is to slightly increase Cys11(I) δ_{con} and slightly decrease the Cys56(IV) δ_{con}, but methanol has an inconsequential effect on the Cys17(III) δ_{con}. The $C_\beta H$ δ_{con} data in Figure 7 reveal that the two forms of the molecule differ systematically in the nature of the magnetic coupling among the three irons, with the *S* form exhibiting more asymmetry (larger spread of

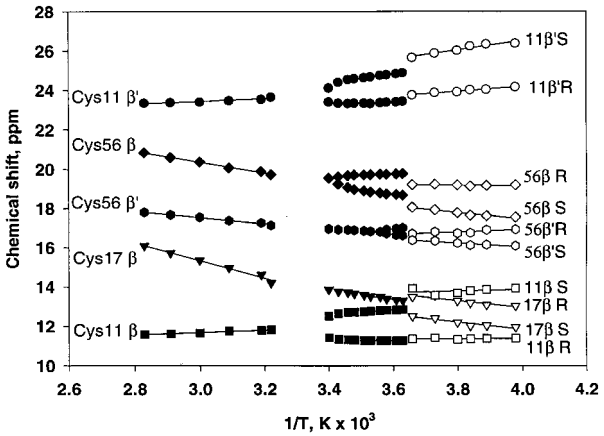

FIGURE 7: Curie plot (observed chemical shift versus reciprocal absolute temperature) for the resolved Cys $C_\beta H$ resonances of *Pf* 3Fe Fd_A^{ox} in H_2O (closed markers) and 70% ^1H_2O/30% CH_3OH (v/v) (open markers). The *R* and *S* components at lower temperatures are labeled as in Figures 3 and 4.

contact shifts) among the three irons than the *R* form. Thus for 3Fe Fd_A^{ox}(*S*-disulfide), Cys11(I) $C_\beta H$s exhibit strong Curie behavior (positive slopes in Figure 7), while both Cys56(IV) and Cys17(III) $C_\beta H$s exhibit strong anti-Curie behavior (negative slopes in Figure 7).

In contrast, 3Fe Fd_A^{ox}(*R*-disulfide) Cys11(I) exhibits smaller δ_{con} than the *S*-form and only weakly Curie-like behavior, while Cys56(IV) $C_\beta H$s display larger δ_{con} than in the *S* form and an essentially temperature-dependent shift. Cys17(III) $C_\beta H$ exhibits a slightly larger δ_{con} and a less steep anti-Curie behavior in the *R* than the S form. It is noteworthy that the mean $\delta_{con}(C_\beta H)$ for the three ligands is essentially the same in 3Fe Fd_A^{ox}(*S*-disulfide) (17.2 ppm at 5 °C in H_2O; 16.8 ppm at −18 °C in 70/30 v/v H_2O/CH_3OH) and 3Fe Fd_A^{ox}(*R*-disulfide) (17.0 ppm at 5 °C in ^1H_2O; 16.7 ppm at −18 °C in H_2O/CH_3OH). Similarly, while the $\delta_{con}(C_\beta H)$ for Cys11(I) and Cys56(IV) differs in water and water/methanol mixed solvent, the mean $\bar{\delta}(C_\beta H)$ at 5 °C is minimally changed (16.9 and 16.7 ppm for *S*, 17.1 and 17.4 ppm for *R*, respectively). These observations indicate that the mean $\langle S_z \rangle$ for the cluster is conserved (*24*, *45*, *56*) but distributed differently among the three irons, depending on the disulfide orientation or presence of methanol.

Thermodynamics and Dynamics of the R/S-Disulfide Isomerism. The low-field Cys11(I) $C_\beta H'$ peak provides the optimum resolution for determining the relative population of the *R* and *S* isomers, where the determination of the relative intensities by simulation reveals intensity ratios ranging from 58:42 at 24 °C to 45:55 at 2 °C (not shown; see Supporting Information). A van't Hoff plot of the ratio of *R* to *S* isomer intensity versus reciprocal absolute temperature yields a straight line (Figure 8) with the thermodynamic parameters $\Delta H = 4.0 \pm 1.2$ kcal/mol (17 ± 5 kJ/mol) and $\Delta S = 14 \pm 2$ cal/(mol·K) [58 ± 10 J/(mol·K)]. Prediction of the *S*/*R* ratio for −18 °C yields 1.8, which is consistent with the relative intensities observed in H_2O/CH_3OH at −18 °C in Figure 6E.

Analysis of the excess line width due to exchange for the Cys11 $C_\beta H'$ peaks, $11\beta'_S$ and $11\beta'_R$, yields a mean exchange rate of 3.2×10^3 s^{-1} at 25 °C, and the Arrhenius and Eyring plots for data in ^1H_2O between 2 and 20 °C yield the activation parameters, $E_a = 10.9 \pm 1.5$ kcal/mol, $\Delta H^\ddagger =$

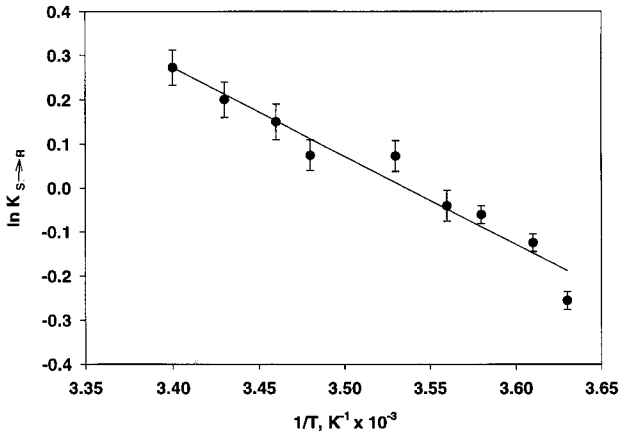

FIGURE 8: Van't Hoff plot of the ratio of the peak intensities for the *R*- to the *S*-disulfide orientation peak of the Cys11(I) $C_\beta H'$ peak as a function of reciprocal absolute temperature for *Pf* 3Fe Fd_A^{ox} in ^1H_2O, 50 mM in phosphate, pH 8.2. The straight line through the points yields $\Delta H = 4.0 \pm 1.2$ kcal/mol and $\Delta S = 14 \pm 5$ cal/(mol·K).

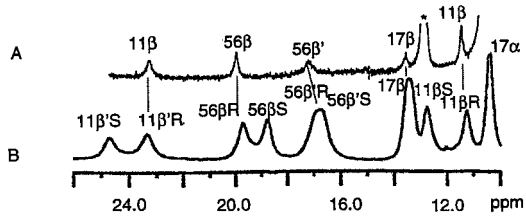

FIGURE 9: Low-field portions of the 600 MHz ^1H NMR spectra of (A) *Pf* 3Fe Fd_A^{ox}(*S*) and Fd_A^{ox}(*R*) and (B) *Pf* 3Fe Fd_B^{ox} with a cleaved disulfide bond, at 10 °C in ^1H_2O, 50 mM in phosphate, pH 8.2. The peak labeled by an asterisk arises from the incompletely converted (*62*) 4Fe form of *Pf* Fd^{ox}.

10.4 ± 1.5 kcal/mol, and $\Delta S^{\ddagger} = -9.4 \pm 4$ cal/(mol·K), respectively.

Effect of Abolishing the Disulfide Bond. The Cys21(V)−Cys48(VI) disulfide in *Pf* Fd can be cleaved (*62*) by dithionite to yield 3Fe Fd_B^{ox}. The resolved portion of the ^1H NMR spectrum of Pf 3Fe Fd_B^{ox} with the cleaved disulfide (*62*) (30% 3Fe Fd_B^{ox} in the presence of 70% 4Fe Fd_B^{ox}) at 10 °C is shown in Figure 9B and can be compared to the two forms of 3Fe Fd_A^{ox} at 10 °C in Figure 9A. It is obvious in Figure 9 that the cluster ligand hyperfine shift pattern for 3Fe Fd_B^{ox} is very similar to that of one of the two resolved isomeric forms of 3Fe Fd_A^{ox}, namely that which is labeled *R* in Figure 4.

DISCUSSION

Effect of Disulfide Orientation on Cluster Magnetic Coupling. Both the $\delta_{con}(C_\beta H)$ and their temperature dependencies differ characteristically in 3Fe Fd_A^{ox}(*S*) and Fd_A^{ox}-(*R*), in a fashion that indicates a difference in the asymmetry of the coupling among the three irons. The observed $\langle S_z \rangle_q$ in eq 1 for each of the three irons, q = a, b, or c, has been modeled using the spin coupling constants *J* in the spin Hamiltonian (*8*, *10*, *45*, *56*):

$$\mathcal{H} = J_{ab}\vec{S}_a\vec{S}_b + J_{ac}\vec{S}_a\vec{S}_b + J_{bc}\vec{S}_b\vec{S}_c \qquad (4)$$

where the relative value of the *J* determines the relative values of $\langle S_z \rangle_q$ and its temperature dependence at each iron, q. However, in the absence of a robust molecular model for

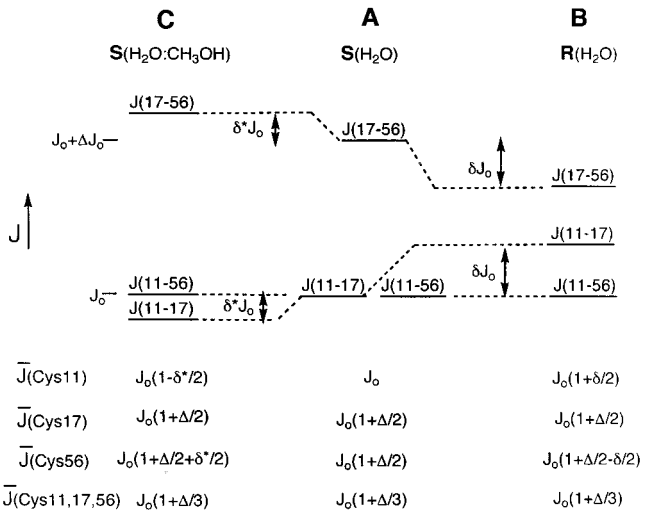

FIGURE 10: Schematic diagram of the relative values of the iron spin−iron coupling constants in *Pf* 3Fe Fd^{ox} as influenced by disulfide orientation and methanol that account for the changes in magnitudes and temperature dependencies of $\delta_{con}(C_\beta H)$ for the three Cys ligands. The reference for these comparisons (*56*), which has $J(11-17) \sim J(11-56) = J_o < J(17-56) = J_o + \Delta J_o$, is the disulfide *S* orientation, as shown in (A), and as either converted to the disulfide *R* orientation (B) or as upon adding methanol (C). The invariant mean $\delta_{con}(C_\beta H)$ indicates a conserved mean *J*. The *J* couplings are changed by δJ upon disulfide reorientation and by $\delta^* J$ upon interaction with methanol.

Pf Fd to obtain $f(\theta)$ in eq 1, only qualitative conclusions can be deduced as to the differences in the asymmetry in the cluster coupling in Fd_A^{ox}(*S*) vs Fd_A^{ox}(*R*).

Modeling the magnitude and temperature dependencies of Cys ligand $\delta_{con}(C_\beta H)$ for the two structurally characterized 3Fe clusters have shown the following (*24*, *45*, *56*): (1) The observed $\delta_{con}(C_\beta H)$ ranges are indicative of a mean *J* value of ~300 cm^{-1}, which, in the limit of three identical *J*s, results in identical $\langle S_z \rangle_q$ for each iron q and low-field $\delta_{con}(C_\beta H)$ with weak anti-Curie behavior for each ligated Cys. (2) The observed differential $\delta_{con}(C_\beta H)$ magnitude and temperature behavior for different Cys ligands can result from asymmetry or differences in the *J* values of as little as 10−20 cm^{-1}, with the general result that the iron with the two largest *J* values exhibits relatively small $\delta_{con}(C_\beta H)$ and *anti-Curie behavior*, while the iron with the two smallest *J* values exhibits relatively large $\delta_{con}(C_\beta H)$ and *Curie-type* behavior. Thus, the case $J_{ab} = J_{ac} = J$, $J_{bc} = J + \Delta J$ leads to Curie behavior for Cys[a] and anti-Curie behavior for Cys[b] and Cys[c], as displayed by the 3Fe cluster of *Dg* (*56*) and *Tl* Fds (*38*). (3) When the symmetry is further lowered such that $J_{ab} < J_{ac} < J_{bc}$, differing by comparable amounts, Cys[a] exhibits Curie, Cys[c] exhibits anti-Curie, and Cys[b] exhibits intermediate (i.e., essential no) temperature dependence (*24*, *45*), as found for the 3Fe cluster of *Rhodopseudomonas palustris* 7Fe Fd (*45*).

Since $f(\theta)$ is not known, specific values of *J* cannot be obtained. However, *changes* in $\delta_{con}(C_\beta H)$ and temperature behavior will indicate which couplings change in which direction. This general information allows us to draw conclusions as to how the spin-coupling topology in 3Fe Fd_A^{ox}(*S*) and Fd_B^{ox}(*S*) differs qualitatively. A simplistic model of the three *J* values is given in part A of Figure 10, which represents the case for Fd_A^{ox}(*S*), where both Cys56(IV) and Cys17(III) exhibit strong anti-Curie and Cys11(I) exhibits

strong Curie behavior (*56*), indicating that, qualitatively, $J_{11-17} \sim J_{11-56} < J_{17-56}$, where $\Delta = J_{17-56} - J_{11-17}$. Upon converting the disulfide to the *R* orientation [i.e., $Fd_A^{ox}(R)$], the mean *J* for the three irons is conserved, since the mean $\delta_{con}(C_\beta H)$ is conserved (Table 1). The decrease in both $\delta_{con}(C_\beta H)$ and Curie slope for Cys11(I), and the increase in $\delta_{con}(C_\beta H)$ and conversion from anti-Curie to non-Curie behavior for Cys56(IV), while the Cys17 $\delta_{con}(C_\beta H)$ shift and temperature slope are changed only a little, demands a decrease in J_{11-56} and a comparable increase in J_{11-17}, while J_{11-56} is largely unchanged, as depicted in part B of Figure 10. Thus the transfer of $\langle S_z \rangle$ from the iron ligated by Cys11(I) to the iron ligated by Cys56(IV) requires small and comparable changes in the *J* values in opposite directions.

It is noteworthy that the effect of disulfide orientation is to alter primarily the *J* couplings of Cys17(III), the residue whose carbonyl oxygen is the acceptor to the Cys21(V) in the disulfide bond (*21*, *29*, *33*). Hence, influences of the disulfide appear to be transmitted directly via the contact between the two chromophores. While it is clear that the orientation of the disulfide bond does modulate the cluster coupling topology, in the absence of a molecular model for either $Fd_A^{ox}(S)$ or $Fd_A^{ox}(R)$ (see below), the detailed structural basis of this difference in spin coupling remains obscure. An important result of this analysis is the recognition that the observed temperature dependence of δ_{con} at elevated temperature (>30 °C) (*44*, *55*), where interconversion between the *S*- and *R*-disulfide orientation is rapid, is only the *average* over the two forms and hence provides insight into the coupling topology of neither of the two forms in solution.

Effect of Methanol on Magnetic Coupling. The effect of methanol addition on the chemical shifts relatively remote from the cluster is negligible, as evidenced by the chemical shift (not shown; see Supporting Information). The effect on the cluster ligand $C_\beta H$ δ_{con} at low temperatures, however, is significant and systematic. The effect of adding methanol at low temperature (10 °C) to $Fd_A^{ox}(S)$ on Cys11(I) is to *increase* $\delta_{con}(C_\beta H)$ by ~0.2−0.4 ppm, *decrease* Cys56(IV) $\delta_{con}(C_\beta H)$ by 0.1−0.4 ppm, but leave Cys17 $\delta_{con}(C_\beta H)$ *minimally altered*, as shown in Figure 7. This influence is exactly the opposite to that observed by converting the *S* to the *R* orientation in H_2O. Again, conserving the mean $\delta_{con}(C_\beta H)$ between water and mixed solvent, and hence mean $\langle S_z \rangle$, suggests changes in J_{11-17} and J_{17-50} as shown in part C in Figure 10. The changes in *J* due to methanol addition are numerically only about one-fourth to one-third of those induced by disulfide orientation.

A more quantitative comparison of the solution structure in H_2O and mixed solvent, which is beyond the scope of the current study, will be necessary to shed light on the nature of the methanol interaction which modulates the coupling. The major advantage of the relatively unperturbed ^1H NMR spectral parameters in the diamagnetic portion of the spectra in mixed solvents at low temperature is that it greatly improves the prospects of time resolving more of the resonances for the *S* and *R* forms and thereby allows the direct investigation by NMR of the difference in molecular structure between $Fd_A^{ox}(S)$ and $Fd_A^{ox}(R)$.

Influence of Cleaving the Disulfide. An earlier analysis of the ^1H NMR spectra of 4Fe Fd_A^{ox} and 3Fe Fd_A^{ox} had shown (*59*) that the peptide NH signals for some dozen residues, most prominently for Cys21, Val24, Lys36, Val37, Lys50, Ala52, and Gln 54, exhibited severe line broadening at low temperature due to the averaging of their very distinct environments in $Fd_A^{ox}(S)$ and $Fd_A^{ox}(R)$. The averaged chemical shifts for these residues, moreover, in contrast to others in the protein, exhibited *large chemical shift differences from the values* in Fd_B^{ox} with the cleaved disulfide bond and displayed highly anomalous temperature gradients (*59*). The temperature gradients of Fd_A^{ox} were such that the shifts for the Fd_A^{ox} averaged over the *S*- and *R*-disulfide orientations *asymptotically approached the shifts in* Fd_B^{ox} *with cleaved disulfide at high temperature, indicating that primarily the R-disulfide orientation is populated at elevated temperature* (*59*). This observation led us to propose that the molecular structure of $Fd_A^{ox}(R)$ is similar to that of Fd_B^{ox} without the disulfide (*59*). This comparison can be further extended here to the cluster.

Comparison of the hyperfine-shifted portions of the ^1H NMR spectrum of the resolved and assigned signals for 3Fe $Fd_A^{ox}(S)$ and 3Fe $Fd_A^{ox}(R)$ at 10 °C in Figure 9A with that for 3Fe Fd_B^{ox} with cleaved disulfide in Figure 9B indeed demonstrates that the cluster contact shifts for 3Fe Fd_B^{ox} are essentially the same as for 3Fe $Fd_A^{ox}(R)$ but distinct from those of 3Fe $Fd_A^{ox}(S)$. Thus both the peptide NH chemical shifts remote from the cluster at high temperature (*59*) and the cluster contact shifts at low temperature confirm a molecular structure for $Fd_A^{ox}(R)$ that is very similar to the homogeneous structure when the disulfide is cleaved. Thus, results suggest that the molecular model for Fd_B^{ox} would assist in unraveling the structural difference between $Fd_A^{ox}(R)$ and $Fd_A^{ox}(S)$. A solution structure determination of *Pf* Fd without a disulfide bond is in planned.

Relationship of Heterogeneity to Function. Analysis of the broadened peptide NHs whose chemical shifts differed significantly between $Fd_A^{ox}(S)$ and $Fd_A^{ox}(R)$ and the pattern of Cys21(V) to Val24 NOESY cross-peak intensities over a temperature range had suggested that, above 90 °C, primarily the $Fd_A^{ox}(R)$ form is populated (*59*). The present determination of the thermodynamic parameter for the disulfide orientational isomerism confirms the conclusion and predicts <15% population of $Fd_A^{ox}(S)$ at >100 °C where the organism thrives (*69*). It thus appears that the structural heterogeneity is not present significantly in the natural environment of *P. furiosus* and hence may not be physiologically relevant. In fact, the unfortunate structural heterogeneity that so severely complicates the determination of the solution structure of *Pf* Fd_A^{ox} at ambient temperature may be largely an artifact of working some 75 °C below the physiological temperature. The determination of a robust molecular model for $Fd_A^{ox}(R)$ is in progress.[2] It is to be noted, however, that since most spectroscopic investigations of Fd are carried out in water below the boiling point (*44*, *55*), great care must be exercised in interpreting the "average" properties of *Pf* Fd_A^{ox} with the alternate disulfide orientation in terms of a single structure.

While only relatively few hyperthermostable proteins have to date been subjected to detailed structural analysis by either X-ray crystallography (*33*, *70*−*74*) or NMR spectroscopy (*21*, *22*, *75*, *76*), no new structural motifs have been observed (for recent reviews, see refs *70*, *71*, and *76*). In particular, the reported structures of other iron−sulfur proteins from hyperthermophiles (*21*, *22*, *33*, *72*−*76*) are remarkably similar to analogous ones from mesophiles. Moreover, the

structures are homogeneous and well defined and give no evidence of equilibrium heterogeneity as detected for *Pf* Fd with intact disulfide bonds (*21*, *40*, *44*, *76*). Hence, it is very unlikely that the *Pf* Fd heterogeneity is directly connected to its extraordinary stability and such heterogeneity should be expected with a greater frequency in proteins from hyperthermophiles than from mesophiles. While the heterogeneity can be detected most reliably by ^{1}H NMR spectroscopy, there is evidence that the *Pf* Fd is also heterogeneous in crystals. Thus, only the cluster of *Pf* Fd is resolved in the crystal structure of *Pf* Fd in a 1:1 complex with its aldehyde oxidoreductase, with the remainder lost due to the disorder introduced by a heterogeneous Fd (*63*).

SUPPORTING INFORMATION AVAILABLE

Three figures showing ^{1}H NMR spectra of *Pf* Fd_A^{ox} in 70% H_2O/30% CH_3OH, a comparison of observed and simulated Cys11 $C_\beta H$ peak area/line width at low temperature, and an Arrhenius plot of $S \Leftrightarrow R$ interconversion. This material is available free of charge via the Internet at http://pubs.acs.org.

REFERENCES

1. Cammack, R. (1992) *Adv. Inorg. Chem. 38*, 281−322.
2. Howard, J. B., and Rees, D. C. (1991) *Adv. Protein Chem. 42*, 199−280.
3. Sticht, H., and Rösch, P. (1998) *Prog. Biophys. Mol. Biol. 70*, 95−136.
4. Middleton, P., Dickson, D. P. E., Johnson, C. E., and Rush, J. D. (1978) *Eur. J. Biochem. 88*, 135−141.
5. Münck, E., Papaefthymiou, V., Surerus, K. K., and Girerd, J. J. (1988) in *Metal clusters in proteins* (Que, L., Ed.) pp 302−325, American Chemical Society, Washington, DC.
6. Noodleman, L. (1991) *Inorg. Chem. 30*, 246−256.
7. Bominaar, E. L., Borshch, S. A., and Girerd, J.-J. (1994) *J. Am. Chem. Soc. 116*, 5362−5372.
8. Noodleman, L., Peng, C. Y., Mouesca, J.-M., and Case, D. A. (1995) *Coord. Chem. Rev. 144*, 199−244.
9. Noodleman, L., Chen, T. L., Case, D. A., Giori, C., Rius, G., Mouesca, J.-M., and Lamotte, B. (1995) in *Nuclear Magnetic Resonance of Paramagnetic Macromolecules* (La Mar, G. N., Ed.) pp 339−367, Kluwer Press, Dordrecht, The Netherlands.
10. Bertini, I., Ciurli, S., and Luchinat, C. (1995) in *Structure and Bonding* (Clarke, M. J., Ed.) pp 1−54, Springer-Verlag, Berlin.
11. Huynh, B. H., Moura, J. J. G., Moura, I., Kent, T. A., Le Gall, J., Xavier, A. V., and Münck, E. (1980) *J. Biol. Chem. 255*, 3242−3244.
12. Mouesca, J. M., Chen, J. L., Noodleman, L., Bashford, D., and Case, D. A. (1994) *J. Am. Chem. Soc. 116*, 11898−11914.
13. Stephens, P. J., Jollie, D. R., and Warshel, A. (1996) *Chem. Rev. 96*, 2491−2513.
14. Achim, C., Bominaar, E. L., and Münck, E. (1998) *J. Biol. Inorg. Chem. 3*, 126−134.
15. Poe, M., Phillips, W. D., McDonald, C. C., and Lovenberg, W. (1970) *Proc. Natl. Acad. Sci., U.S.A. 65*, 797−804.
16. Bertini, I., Turano, P., and Vila, A. J. (1993) *Chem. Rev. 93*, 2833−2933.
17. Cheng, H., and Markley, J. L. (1995) *Annu. Rev. Biophys. Biomol. Struct. 24*, 209−237.
18. Goodfellow, B. J., and Macedo, A. L. (1999) in *Reports on NMR Spectroscopy*, pp 119−177, Academic Press, London.
19. Bertini, I., Donaire, A., Feinberg, B. A., Luchinat, C., Piccioli, M., and Yuan, H. (1995) *Eur. J. Biochem. 232*, 192−205.
20. Bertini, I., Luchinat, C., and Rosato, A. (1996) *Prog. Biophys. Mol. Biol. 66*, 43−80.
21. Wang, P. L., Donaire, A., Zhou, Z. H., Adams, M. W. W., and La Mar, G. N. (1996) *Biochemistry 35*, 11319−11328.
22. Sticht, H., Wildegger, G., Bentrop, D., Darimont, B., Sterner, R., and Rösch, P. (1996) *Eur. J. Biochem. 237*, 726−735.
23. Davy, S. L., Osborne, M. J., and Moore, G. R. (1998) *J. Mol. Biol. 277*, 683−706.
24. Aono, S., Bertini, I., Cowan, J. A., Luchinat, C., Rosato, A., and Viezzoli, M. S. (1996) *J. Biol. Inorg. Chem. 1*, 523−528.
25. Bertini, I., Luchinat, C., and Rosato, A. (1999) *Adv. Inorg. Chem. 47*, 251−282.
26. Goodfellow, B. J., Macedo, A. L., Rodrigues, P., Moura, I., Wray, V., and Moura, J. J. G. (1999) *J. Biol. Inorg. Chem. 4*, 421−430.
27. Fukuyama, K., Matsubara, H., Tsukihara, T., and Katsube, Y. (1989) *J. Mol. Biol. 210*, 383−398.
28. Backes, G., Mino, Y., Loehr, T., Meyer, T., Cusanovich, M., Sweeney, W., Adman, E., and Sanders-Loehr, J. (1991) *J. Am. Chem. Soc. 113*, 2055−2064.
29. Kissinger, C. R., Sieker, L. C., Adman, E. T., and Jensen, L. H. (1991) *J. Mol. Biol. 219*, 693−715.
30. Stout, C. D. (1993) *J. Biol. Chem. 268*, 25920−25927.
31. Séry, A., Housset, D., Serre, L., Bonicel, J., Hatchikian, C., Frey, M., and Roth, M. (1994) *Biochemistry 33*, 15408−15417.
32. Duée, E. D., Fanchon, E., Vicat, J., Sieker, L. C., Meyer, J., and Moulis, J.-M. (1994) *J. Mol. Biol. 243*, 683−695.
33. Macedo-Ribeiro, S., Darimont, B., Sterner, R., and Huber, R. (1996) *Structure 4*, 1291−1301.
34. Moulis, J. M., Sieker, L. C., Wilson, K. S., and Dauter, Z. (1996) *Protein Sci. 5*, 1765−1775.
35. Dauter, Z., Wilson, K. S., Sieker, L. C., Meyer, J., and Moulis, J. M. (1997) *Biochemistry 36*, 16065−16073.
36. Macedo, A. L., Palma, P. N., Moura, I., LeGall, J., Wray, V., and Moura, J. J. G. (1993) *Magn. Reson. Chem. 31*, S59−S67.
37. Bertini, I., Capozzi, F., Luchinat, C., Piccioli, M., and Vila, A. J. (1994) *J. Am. Chem. Soc. 116*, 651−660.
38. Donaire, A., Gorst, C. M., Zhou, Z. H., Adams, M. W. W., and La Mar, G. N. (1994) *J. Am. Chem. Soc. 116*, 6841−6849.
39. Scrofani, S. D. B., Brereton, P. S., Hamer, A. M., Lavery, M. J., McDowall, S. G., Vincent, G. A., Brownlee, R. T. C., Hoogenraad, N. J., Sadek, M., and Wedd, A. G. (1994) *Biochemistry 33*, 14486-14495.
40. Gorst, C. M., Yeh, T., Teng, Q., Calzolai, L., Zhou, J. H., Adams, M. W. W., and La Mar, G. N. (1995) *Biochemistry 34*, 600−610.
41. Calzolai, L., Gorst, C. M., Zhao, Z. H., Teng, Q., Adams, M. W. W., and La Mar, G. N. (1995) *Biochemistry 34*, 11373−11384.
42. Wildegger, G., Bentrop, D., Ejchart, A., Alber, M., Hage, A., Sterner, R., and Rösch, P. (1995) *Eur. J. Biochem. 229*, 658−668.
43. Lebrun, E., Simenel, C., Guerlesquin, F., and Delepierre, M. (1996) *Magn. Reson. Chem. 34*, 873−880.
44. Calzolai, L., Gorst, C. M., Bren, K. L., Zhou, Z. H., Adams, M. W. W., and La Mar, G. N. (1997) *J. Am. Chem. Soc. 119*, 9341−9350.
45. Bertini, I., Dikiy, A., Luchinat, C., Macinai, R., Viezzoli, M. S., and Vincenzini, M. (1997) *Biochemistry 36*, 3570−3579.
46. Kyritsis, P., Kümmerle, R., Huber, J. G., Gaillard, J., Guigliarelli, B., Popescu, C., Münck, E., and Moulis, J.-M. (1999) *Biochemistry 38*, 6335−6345.
47. Bertini, I., and Luchinat, C. (1996) *Coord. Chem. Rev. 150*, 1−296.
48. Davy, S. L., Osborne, M. J., Breton, J., Moore, G. R., A. J., T., Bertini, I., and Luchinat, C. (1995) *FEBS Lett. 363*, 199−204.
49. Bentrop, D., Bertini, I., Luchinat, C., Nitschke, W., and Muhlenhoff, U. (1997) *Biochemistry 36*, 13629−13637.
50. Antonkine, M. L., Bentrop, D., Bertini, I., Luchinat, C., Shen, G., Bryant, D. A., Stehlik, D., and Golbeck, J. H. (2000) *J. Biol. Inorg. Chem. 5*, 381−392.
51. Bertini, I., Luchinat, C., Mincione, G., and Sorieino, A. (1998) *Inorg. Chem. 137*, 969−972.
52. Macedo, A. L., Rodrigues, P., and Goodfellow, B. J. (1999) *Coord. Chem. Rev. 190−192*, 871−881.

53. Nagayama, K., Ohmori, D., Imai, T., and Oshima, T. (1986) in *Iron−Sulfur Protein Research* (Matsubara, H., Ed.) pp 125−138, Japan Science Society Press, Tokyo.
54. Cheng, H., Grohmann, K., and Sweeney, W. (1992) *J. Biol. Chem. 267*, 8073−8080.
55. Busse, S. C., La Mar, G. N., Yu, L. P., Howard, J. B., Smith, E. T., Zhou, Z. H., and Adams, M. W. W. (1992) *Biochemistry 31*, 11952−11962.
56. Macedo, A. L., Moura, I., Moura, J. J. G., LeGall, J., and Huynh, B. H. (1993) *Inorg. Chem. 32*, 1101−1105.
57. Aono, S., Bryant, F. O., and Adams, M. W. W. (1989) *J. Bacteriol. 171*, 3433−3439.
58. Teng, Q., Zhou, Z. H., Smith, E. T., Busse, S. C., Howard, J. B., Adams, M. W. W., and La Mar, G. N. (1994) *Biochemistry 33*, 6316−6326.
59. Wang, P.-L., Calzolai, L., Bren, K. L., Teng, Q., Jenney, F. E., Jr., Brereton, P. S., Howard, J. B., Adams, M. W. W., and La Mar, G. N. (1999) *Biochemistry 38*, 8167−8178.
60. Calzolai, L., Zhou, Z. H., Adams, M. W. W., and La Mar, G. N. (1996) *J. Am. Chem. Soc. 118*, 2513−2514.
61. Conover, R. C., Park, J.-B., Adams, M. W. W., and Johnson, M. K. (1990) *J. Am. Chem. Soc. 112*, 4562−4564.
62. Gorst, C. M., Zhou, Z.-H., Ma, K., Teng, Q., Howard, J. B., Adams, M. W. W., and La Mar, G. N. (1995) *Biochemistry 34*, 8788−8795.
63. Yu, L., Faham, S., Roy, R., Adams, M. W. W., and Rees, D. C. (1999) *J. Mol. Biol. 286*, 899−914.
64. Brereton, P. S., Verhagen, F. J. M., Zhou, J. H., and Adams, M. W. W. (1998) *Biochemistry 37*, 7351−7362.
65. Jeener, J., Meier, B. H., Bachmann, P., and Ernst, R. R. (1979) *J. Chem. Phys. 71*, 4546−4553.
66. Bax, A., and Davis, D. G. (1985) *J. Magn. Reson. 65*, 355−260.
67. Sandström, J. (1982) *Dynamic NMR Spectroscopy*, Academic Press, New York.
68. Bain, A. D., and Duns, G. J. (1995) *J. Magn. Reson. 112*, 258.
69. Fiala, G., and Stetter, K. O. (1986) *Arch. Microbiol. 145*, 56−61.
70. Rees, D. C. (2001) in *Methods in Enzymology* (Adams, M. W. W., and Kelly, R. M., Eds.) pp 423−437, Academic Press, San Diego.
71. Petsko, G. A. (2001) in *Methods in Enzymology* (Adams, M. W. W., and Kelly, R. M., Eds.) pp 469−478, Academic Press, San Diego.
72. Day, M. W., Hsu, B. T., Joshua-Tor, L., Park, J.-B., Zhou, Z. H., Adams, M. W. W., and Rees, D. C. (1992) *Protein Sci. 1*, 1494−1507.
73. Fujii, T., Hata, Y., Wakagi, T., Tanaka, N., and Oshima, T. (1996) *Nat. Struct. Biol. 3*, 834−836.
74. Bau, R., Rees, D. C., Jr., D. M. K., Scott, R. A., Huang, H., Adams, M. W. W., and Eidsness, M. K. (1998) *J. Biol. Inorg. Chem. 3*, 484−493.
75. Blake, P. R., Park, J.-B., Zhou, Z. H., Hare, D. R., Adams, M. W. W., and Summers, M. F. (1992) *Protein Sci. 1*, 1508−1521.
76. La Mar, G. N. (2001) in *Methods in Enzymology* (Adams, M. W. W., and Kelly, R. M., Eds.) pp 351−389, Academic Press, San Diego.

BI0106179